A New Differential Magnetic-Field Probe With Parasitic Elements for Near-Field Scanning

Lei Wang, Xiaoxian Liu, Guoguang Lu, and Zhangming Zhu

***Abstract*—Herein, A new differential magnetic-field probe with parasitic elements is presented. The proposed probe has two pairs of shorted differential loops as parasitic elements, which could enhance the detection sensitivity owing to the increased detection area. The proposed probe comprises a U-shaped loop with two outputs as the driven element, two pairs of shorted differential loops as parasitic elements, a pair of shorted via, a pair of connected via, and many shielded vias. First, the usual single-loop probe is theoretically studied. Second, a pair of shorted loops is inserted into the differential single-loop probe as a parasitic element to receive more magnetic flux. Third, another pair of shorted loops is etched into the probe to further improve the detection sensitivity. The corresponding simulation results are presented to prove the effectiveness of the design. Finally, the proposed probe with parasitic elements is designed, printed, and evaluated. Measurement results reveal that the designed probe has high detection sensitivity.**

***Index Terms*—Detection sensitivity, differential probe, near-field scanning.**

I. Introduction

With respect to the electromagnetic interference (EMI) of high-speed electronic systems, the near-field canning method is one of the most popular solutions for locating the EMI source [1], [2], [3], [4]. The corresponding descriptions have been given in international standards (TS 62132 and IEC 61967) [5], [6]. As the core element of the measurement system, near-field probes have been extensively studied in [7], [8], [9], [10]. These probes are characterized by: wideband operation [11], [12], multiple components [13], [14], [15], [16], high-spatial resolution [17], [18], [19], [20], high electric-field suppression [21], [22], [23], [24], and high-sensitivity [25], [26], [27], [28], [29], [30], [31], [32], [33], [34], [35]. To improve the performance of a probe, several of the most popular approaches are as follows: first, the bandwidth of the probe can be expanded to 30 GHz by introducing a coax-thru-hole via array to tune impedance matching [11]. Second, when multiple orthogonal loops are used to sense the electromagnetic field, a composite probe can simultaneously test multiple field components [16]. Third, it is well known that the smaller the detection aperture, the higher the spatial-resolution [20]. Fourth, some shield vias are utilized to improve the electric-field suppression ratio by preventing undesired electric-field coupling [24]. Electric field suppression ratios should be >21 dB for frequencies up to 14 GHz. Finally, the sensitivity of the probe can be increased by loading LC resonant circuits [25], [26], [27], [28] and active amplifiers [29], [30], [31] in the probe. Usually, LC resonant circuits are used to excite a LC resonant frequency point to sense more RF signals, while active amplifiers are utilized to amplify the measured RF signals. However, the operational bandwidths of these active amplifiers and LC resonant circuits are always very narrow and operate near 1.575 GHz, limiting the application of the high-sensitivity probe. Therefore, it is urgent to develop a new differential probe with high detection sensitivity. Recently, differential probes with two output ports [32], [33], [34], [35] are massively studied to improve the operation performance. A pair of differential loops [32], [33] and a U-shaped loop [34], [35] are introduced into the probes to achieve high detection sensitivity and multiple-component measurements, respectively.

Based on the usual single-loop probe, a new differential magnetic-field probe with high detection sensitivity is proposed herein. The presented probe includes a U-shaped loop with two outputs as the driven element, two pairs of shorted differential loops as parasitic elements, a pair of shorted vias, a pair of connected vias, and many shielded vias. Herein, a theoretical investigation of the conventional single-loop probe is first presented. Subsequently, a pair of shorted loops as a parasitic element is inserted into the differential single-loop probe to receive additional magnetic flux. Moreover, another pair of shorted loop as parasitic elements is also added into the proposed probe to enhance the detection sensitivity. By employing these shorted loops with the U-shaped differential loop, the detection sensitivity of the proposed probe could be clearly enhanced. The remaining article is organized as follows: the geometry of the probe is depicted in Section II. The probe operational mechanism is presented in Section III. Simulation and measurement results are given in Section IV. Finally, the conclusion is discussed in Section V.

II. Probe Design

First, a seven-layered printed circuit board (PCB) is used to print the proposed probe (Fig. 1). The PCB comprises two

Manuscript received 8 February 2024; revised 8 April 2024; accepted 16 April 2024. Date of publication 29 April 2024; date of current version 6 May 2024. *(Corresponding author: Guoguang Lu.)*

Lei Wang is with the School of Microelectronics, Xidian University, Xi'an, Shaanxi 710071, China, and also with the Science and Technology on Reliability Physics and Application of Electronic Component Laboratory, China Electronic Product Reliability and Environmental Testing Research Institute, Guangzhou 511370, China (e-mail: leiwang@ceprei.com).

Xiaoxian Liu and Zhangming Zhu are with the School of Microelectronics, Xidian University, Xi'an, Shaanxi 710071, China (e-mail: liudou132@163.com; zmyh@263.net).

Guoguang Lu is with the Science and Technology on Reliability Physics and Application of Electronic Component Laboratory, CEPREI, Guangzhou 511370, China (e-mail: luguog@126.com).

Digital Object Identifier 10.1109/JPHOT.2024.3391012

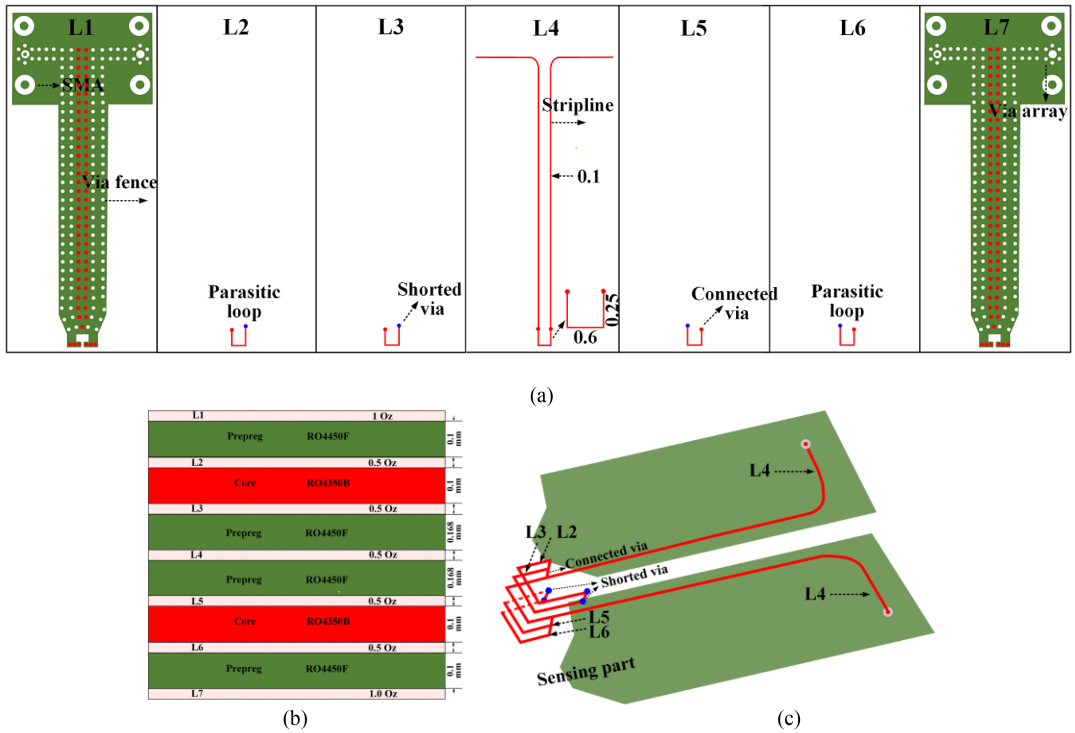

Fig. 1. Geometry of the proposed probe. (a) Top view of each layer. (b) Stack-up. (c) 3-D view.

Rogers 4450F with a thickness of 0.1 mm, two Rogers 4350B with a thickness of 0.1 mm, and two Rogers 4450F with a thickness of 0.168 mm. The size of the detection loop in Probe B is 0.6 mm × 0.25 mm. In the proposed probe, the U-shaped loop is etched on the center of the PCB (layer L4), the shorted loops are printed on layers L2, L3, L5, and L6, and the ground planes are etched on layers L1 and L7. Notably, two connected vias are used to connect L2 and L3 to L4, and L5 and L6 to L4, and two shorted vias are utilized to connect the L2, L3, L5, and L6 to ground planes. Therefore, the parasitic loops can not only be connected to the U-shaped loop but also be grounded by connecting to the ground planes. A pair of 2.92mm vertical compression-mount precision test connectors are employed to adjust impedance matching. In addition, some shield vias and via fences are used to reject unwanted electric-field coupling and suppress the undesired parallel-plate modes [35]. The stack-up geometry, the details of each layer and a three-dimensional view are shown in Fig. 1(a)–(c), respectively.

III. Operational Mechanism

A. Sensitivity Enhancement Mechanism

The single-loop probe has already been designed and studied in [31], [32]. Unlike the usual differential single-loop probes that can only sense a small amount of magnetic flux, the proposed probe with parasitic loops can sense more magnetic flux. For explaining the operational principle, the differential single-loop and parasitic loops are given together in Fig. 2. When these loops are placed at $\theta = 0°$, the outputs (I_{ez}) of the electric-field coupling at two ports are of equal amplitude and in phase, while the outputs (I_{hx}) of the magnetic-field coupling are of equal

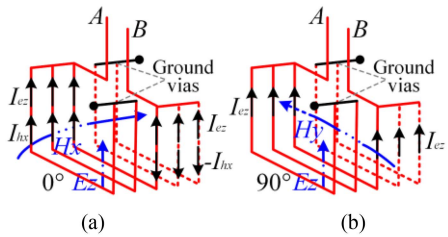

Fig. 2. Operating mechanism of the proposed probe with different placements, (a) $\theta = 0°$, and (b) $\theta = 90°$.

amplitude and in antiphase. We can get,

$$I_A = 3\left(I_{hx} + I_{ez}\right) \tag{1}$$

$$I_B = 3\left(-I_{hx} + I_{ez}\right) \tag{2}$$

This implies that using differential- and common-mode operations, the electric- and magnetic-fields entering the loops are separately extracted, as follows:

$$I_{ez} = \frac{I_A + I_B}{6} \tag{3}$$

$$I_{hx} = \frac{I_A - I_B}{6} \tag{4}$$

However, when these loops are placed at $\theta = 90°$, the I_{ez} values at two ports are equal in phase and I_{hx} values entering the differential dual loops is zero.

$$I_A = I_B = 3I_{ez} \tag{5}$$

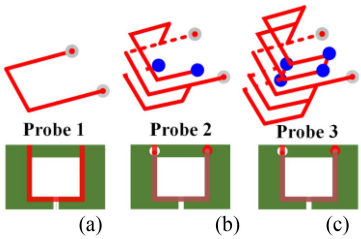

Fig. 3. Structures of three evolutional probes. (a) Probe 1. (b) Probe 2. (c) Probe3.

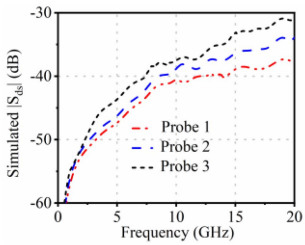

Fig. 4. The simulated $|S_{ds}|$ of three evolutional probes.

In addition, when the sizes of the loop are small enough, we can find that the electric-field coupling values at $\theta = 0°$ and 90° are almost equal. Finally, as shown in Fig. 2, the magnetic fluxes entering into the proposed probe are three times than that of the usual differential single-loop, which means that the detection sensitivity of the proposed probe can be enhanced.

B. Three Evolutional Probes

In this part, three evolutional probes including single-loop probe (Probe 1), single-loop probe with a pair of shorted loops, (Probe 2), and single-loop probe with two pairs of shorted loops (Probe 3) are used to characterize the function of the shored differential loops as parasitic elements (Fig. 3). Notably, $|S_{ds}| = (|S_{21}| - |S_{31}|)/\sqrt{2}$ represents the magnetic-field coupling of these probes in the simulation model. Thus, the corresponding simulation $|S_{ds}|$ values are given and studied in Fig. 4. Notably, the simulation $|S_{ds}|$ values of Probe 2 is greater than that of Probe 1, which means more magnetic flux can be sensed by Probe 2 owing to the existence of a pair of shorted differential loops. Besides, upon comparing these simulation $|S_{ds}|$ values between Probes 2 and 3, we find that the simulation $|S_{ds}|$ of the proposed probe (Probe 3) is greater than that of Probe 2, which means that the simulation $|S_{ds}|$ of the proposed probe is increased owing to the existence of an additional pair of shorted differential loops. Therefore, utilization of the differential loops can lead to the sensing of more magnetic flux, improving the probe sensitivity. In addition, combining the above simulation results, we can easily draw a conclusion that with increasing of parasitic loops, the simulation $|S_{ds}|$ increases. However, this conclusion is based on the ideal state. In fact, the increase in $|S_{ds}|$ not sustainable because of the influence of uncontrollable parasitic effects, such as connect and shield via, etc. Finally,

TABLE I
COMPARISON BETWEEN THE DESIGNED AND PUBLISHED MAGNETIC-PROBES

Probes	Detection loop (mm^2)	Detection structure	Layers	Detection sensitivity	Working frequency
[11]	0.5 × 0.7	Shorted loop	four	low	Up to 10 GHz
[12]	1.0 ×2.0	Shorted loop	five	low	Up to 6 GHz
[13]	1.2 × 0.4	Shorted loop	three	low	Up to 30 GHz
[32]	0.3 × 0.6	Differential loops	four	high	Up to 14 GHz
[33]	1.2 × 0.6	Differential loops	four	high	Up to 10 GHz
[34]	1.16 × 1.39	Single loop	four	Low	Up to 12GHz
[35]	0.6 × 0.6	Single loop + a pair of U-shaped long loops	five	high	Up to 14GHz
Proposed	0.60 × 0.25	Single loop + two pairs of grounded loops	Seven	High	Up to 16GHz

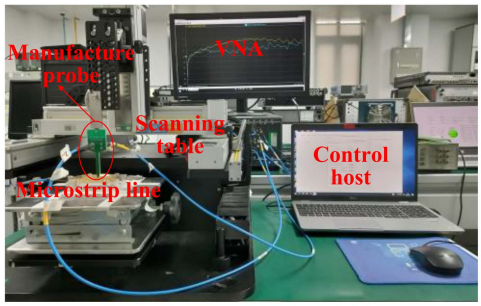

(a)

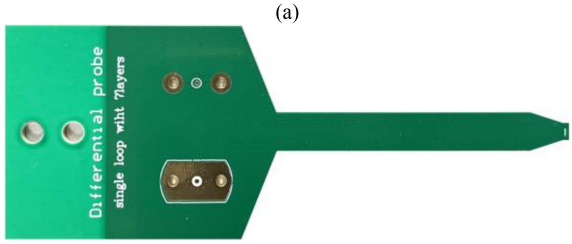

(b)

Fig. 5. Pictures of the measurement system and the manufactured probe. (a) Measurement system. (b) Manufactured probe.

a comparison between the designed and published magnetic-probes is given in Table I. As shown, the designed probe has high detecion sensitivity and wide operational bandwidth.

IV. PROBE CHARACTERISTIC

A. Measurement Setup

To demonstrate the design rationality, the proposed probe is printed and measured. Usually, the probe can be measured and characterized by using a straight microstrip line and near-field scanning system, which has been reported in IEC 61967-3 [6]. A sketch map of the measurement system and the manufactured probe are presented in Fig. 5. As depicted, the measurement system comprises six-port Keysight M9804A VNA as an excitation and receiver, a near-field scanning table with a control host as

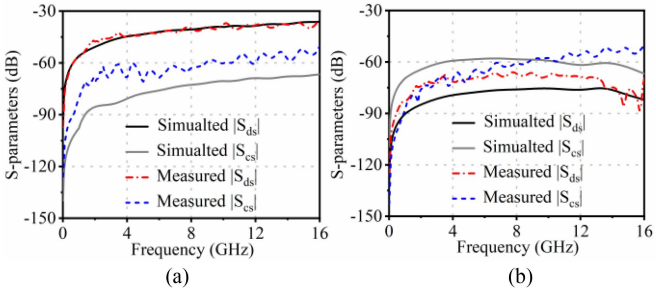

Fig. 6. Simulated and measured *S*-parameters of the proposed probe with different placements, (a) $\theta = 0°$, and (b) $\theta = 90°$.

a mover, a 50-Ω microstrip line as the calibration kit, and the probe as an induction device. Notably, Port 1 of the VNA is connected to one end of the microstrip line, while Ports 2 and 3 are connected to two outputs of the probe. In addition, the other end of the microstrip line is terminated to a 50-Ω match load. The 50-Ω microstrip line with a width of 1.7 mm is etched onto a large substrate RO4350B with dimensions of 80 × 42 × 0.762 mm^3. The distance from the bottom of the probe to the upper surface of the microstrip line is 1mm. In addition, the magnetic- and electric-field couplings from the microstrip line to the probe are presented by differential- and common-mode transmission coefficients $|S_{ds}| = (|S_{21}| - |S_{31}|)/\sqrt{2}$ and $|S_{cs}| = (|S_{21}| + |S_{31}|)/\sqrt{2}$, respectively. At last, in order to further verify the accuracy of measurement results, the simulation model is also given and simulated, which consists of the microstrip line model and the probe model.

B. Frequency Response

Notably, the measurement $|S_{ds}|$ (dB) values cannot not directly represent the actual magnetic-field values, they must be converted. This conversation process is regarded as calibration. According to the previous study in [27], the calibrate factor (CF) can be calculated as follows:

$$\begin{aligned} |CF_h| &= \left|\frac{H}{V_{outh}}\right| \\ &= 20\log_{10}\left[\frac{h}{\pi d\,(d+2h)}\right] \\ &\quad - |S_{ds}| - 34\,[\text{dB}.\,(A/m)\,/V] \end{aligned} \tag{6}$$

where the units of h, d, $|CF_h|$, and $|S_{ds}|$ are m, dB·S/m, and dB, respectively. The d is the distance from the upper layer of the microstrip line to the center of the detection part, while the d is the thickness of the microstrip line. In this measurement, d and h are equal to 1.425 and 0.762 mm, respectively. Thus, the actual magnetic field can be obtained using the equation $V_{outh}\cdot|CF_h|$. Fig. 6 presents the simulation and measurement $|S_{ds}|$ and $|S_{cs}|$ of the proposed probe, respectively, with different phases. As can be seen, the simulation $|S_{ds}|$ values are greater than the simulation $|S_{cs}|$ values at $\theta = 0^\circ$, and the simulation $|S_{cs}|$ values are relatively small at $\theta = 0^\circ$ and 90°, indicating that the proposed probe can receive magnetic-field components at $\theta = 0^\circ$. Additionally, the simulation $|S_{cs}|$ values are always less than the measurement $|S_{cs}|$ values. This is because the thickness of the signal line is set to zero in the simplified simulation model. However, the thickness of the signal line exhibits a clear impact on the electric-field coupling in the actual probe. Finally, Fig. 7 gives the simulation and test CF curves of the proposed probe with frequency variation. There is a good agreement between the simulated and measured results.

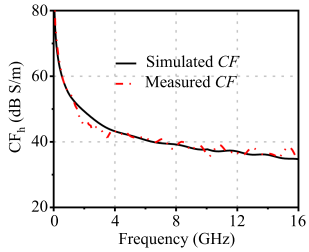

Fig. 7. Simulated and tested *CFs* of the proposed probe.

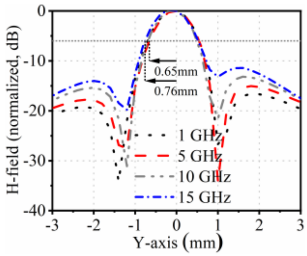

Fig. 8. Measured frequency response as a function of position for the proposed probe with different positions with $\theta = 0^\circ$.

C. Spatial Resolution

To study the capability of recognizing EMI traces, spatial resolution is defined in IEC 61967-6. Usually, the spatial resolution can be measured by placing probes at $\theta = 0^\circ$, and then moving across the microstrip line. The measured amplitude responses of the proposed probe with different positions at $\theta = 0^\circ$ from 1 to 15 GHz are presented in Fig. 8, and the measured amplitude responses are normalized by the maximum values at a special position. According to a previous study [35], the spatial resolution is characterized as the distance between the -6dB level on the response curve and the maximum response. As depicted, the measured spatial resolution of the proposed probe is in the range of 0.65 to 0.76 mm for frequencies from 1 to 15 GHz in the y-direction.

V. Conclusion

Herein, A new differential magnetic-field probe with parasitic elements is presented. The proposed probe has two pairs of shorted differential loops as parasitic elements, which could substantially enhance the detection sensitivity owing to the increased detection area. The proposed probe comprises a U-shaped loop with two outputs as the driven element, two pairs of shorted

via, a pair of connected via, and many shielded vias. First, the usual single-loop probe is theoretically studied. Second, a pair of shorted loops is inserted into the differential single-loop probe as a parasitic element to receive more magnetic flux. Third, another pair of shorted loops is etched into the probe to further improve the detection sensitivity. The corresponding simulation results are presented to prove the effectiveness of the design. Finally, the proposed probe with parasitic elements is designed, printed, and evaluated. Measurement results reveal that the designed probe has high detection sensitivity.

REFERENCES

[1] D. Baudry, C. Arcambal, A. Louis, B. Mazari, and P. Eudeline, "Applications of the near-field techniques in EMC investigations," *IEEE Trans. Electromagn. Compat.*, vol. 49, no. 3, pp. 485–493, Aug. 2007.

[2] J. Zhang, K. W. Kam, J. Min, V. V. Khilkevich, D. Pommerenke, and J. Fan, "An effective method of probe calibration in phase-resolved near- fifield scanning for EMI application," *IEEE Trans. Instrum. Meas.*, vol. 62, no. 3, pp. 648–658, Mar. 2013.

[3] G.-H. Li, W. Huang, and D. Pommerenke, "Effect of cooling on the probe system sensitivity for low signal strength RFI problems," in *Proc. IEEE Int. Symp. Electromagn. Compat.*, 2013, pp. 134–137.

[4] Q. Huang, F. Zhang, T. Enomoto, J. Maeshima, K. Araki, and C. Hwang, "Physics-based dipole moment source reconstruction for RFI on a practical cellphone," *IEEE Trans. Electromagn. Compat.*, vol. 59, no. 6, pp. 1693–1700, Dec. 2017.

[5] "Integrated circuits - Measurement of electromagnetic immunity - Part 9: Measurement of radiated immunity-Surface scan method," IEC, Geneva, Switzerland, Tech. Specification 62132-9, 2014.

[6] "Integrated circuits-Measurement of electromagnetic emissions,150KHz to 1GHz-Part3: Measurement of radiated emissions-surface scan method," IEC, Geneva, Switzerland, Tech. Specification 61967-3, 2005.

[7] M. Ramdani et al., "The electromagnetic compatibility of integrated circuits—Past, present, and future," *IEEE Trans. Electromagn. Compat.*, vol. 51, no. 1, pp. 78–100, Feb. 2009.

[8] W. Fang et al., "Noncontact RF voltage sensing of a printed trace via a capacitive-coupled probe," *IEEE Sensors J.*, vol. 18, no. 21, pp. 8873–8882, Nov. 2018.

[9] Z. Ren, M. S. Boybay, and O. M. Ramahi, "Near-field probes for subsurface detection using split-ring resonators," *IEEE Trans. Microw. Theory Techn.*, vol. 59, no. 2, pp. 488–495, Feb. 2011.

[10] N. N. Mai-Khanh, T. Iizuka, M. Yamada, O. Morita, and K. Asada, "An integrated high-precision probe system in 0.18-μm CMOS for near-field magnetic measurements on cryptographic LSIs," *IEEE Sensors J.*, vol. 13, no. 7, pp. 2675–2682, Jul. 2013.

[11] Z. Yan, W. Liu, J. Wang, D. Su, X. Yan, and J. Fan, "Noncontact wideband current probes with high sensitivity and spatial resolution for noise location on PCB," *IEEE Trans. Instrum. Meas.*, vol. 67, no. 12, pp. 2881–2891, Dec. 2018.

[12] N. Tamaki, N. Masuda, T. Kuriyama, J.-C. Bu, M. Yamaguchi, and K. -I. Arai, "A miniature thin-film shielded-loop probe with a flip-chip bonding for magnetic near field measurement," *IEICE Trans. Electron.*, vol. J87-C, no. 3, pp. 335–342, Mar. 2004.

[13] L. Wang, Y. En, and Z. Zhu, "A ultrawideband multi-component differential magnetic probe for near-field scanning," *IEEE Trans. Circuits Syst. II: Exp. Briefs*, vol. 69, no. 11, pp. 4323–4328, Nov. 2022.

[14] L. Wang, X. Liu, Y. En, and Z. Zhu, "A composite probe capable of simultaneously measuring two orthogonal magnetic-fields," *IEEE Trans. Circuits Syst. II: Exp. Briefs*, vol. 70, no. 2, pp. 521–525, Feb. 2023.

[15] L. Wang, Y. En, and Z. Zhu, "A broadband multicomponent magnetic probe with improved electric-field suppression performance," *IEEE Sensors J.*, vol. 23, no. 6, pp. 5920–5926, Mar. 2023.

[16] L. Wang, Y. En, and Z. Zhu, "An ultrawideband differential magnetic-field probe for near-field scanning," *IEEE Microw. Wireless Technol. Lett.*, vol. 33, no. 2, pp. 224–227, Feb. 2023.

[17] Y.-T. Chou and H.-C. Lu, "Space difference magnetic near-field probe with spatial resolution improvement," *IEEE Trans. Microw. Theory Techn.*, vol. 61, no. 12, pp. 4233–4244, Dec. 2013.

[18] O. Malyuskin and V. F. Fusco, "High-resolution microwave near-field surface imaging using resonance probes," *IEEE Trans. Instrum. Meas.*, vol. 65, no. 1, pp. 189–200, Jan. 2016.

[19] M. A. Abou-Khousa, K. T. Muhammed Shafi, and X. Xingyu, "High-resolution UHF near-field imaging probe," *IEEE Trans. Instrum. Meas.*, vol. 67, no. 10, pp. 2353–2362, Oct. 2018.

[20] R. Yang, X.-C. Wei, Y.-F. Shu, and Y.-B. Yang, "A High-frequency and high spatial resolution probe design for EMI prediction," *IEEE Trans. Instrum. Meas.*, vol. 68, no. 8, pp. 3012–3019, Aug. 2019.

[21] W. Shao et al., "Systematic characterization of dual probes for electromagnetic near-field measurement," *IEEE Sensors J.*, vol. 21, no. 4, pp. 4713–4722, Feb. 2021.

[22] Y.-T. Chou and H.-C. Lu, "Magnetic near-field probes with high-passand notch filters for electric field suppression," *IEEE Trans. Microw. Theory Techn.*, vol. 61, no. 6, pp. 2460–2470, Jun. 2013.

[23] S. Yang, Q. Huang, G. Li, R. Zoughi, and D. J. Pommerenke, "Differential E-field coupling to shielded H-field probe in near-field measurements and a suppression approach," *IEEE Trans. Instrum. Meas.*, vol. 67, no. 12, pp. 2872–2880, Dec. 2018.

[24] X. He, X.-C. Li, Z.-H. Peng, Y.-X. Liu, and J.-F. Mao, "An ultrawideband magnetic probe with high electric field suppression ratio," *IEEE Trans. Instrum. Meas.*, vol. 70, 2021, Art. no. 8005309.

[25] Z.-P. Chen, Z.-G. Liu, S. Zhang, M.-Z. Li, and W.-B. Lu, "An enhanced-sensitivity tangential electric field probe with tunable resonant frequency," *IEEE Trans. Instrum. Meas.*, vol. 72, 2023, Art. no. 8003212.

[26] L. Dou, S. Sui, and Y. Cui, "Resonant measurement of coaxial probe based on tunable impedance matching network," *IEEE Microw. Wireless Technol. Lett.*, vol. 33, no. 6, pp. 763–766, Jun. 2023..

[27] Y. Lu, F. Tong, C. Gu, L.-S. Wu, and J.-F. Mao, "A near-field motion detection technique based on a resonant magnetic probe," *IEEE Sensors Lett.*, vol. 6, no. 4, Apr. 2022, Art. no. 3500904.

[28] Y. Lu, L. Wen, C. Gu, L.-S. Wu, and J.-F. Mao, "A high-sensitivity magnetic-field resonant probe based on embedded stripline structure," in *Proc. IEEE Topical Conf. Wireless Sensors Sensor Netw.*, 2022, pp. 1–4.

[29] X. He, X.-C. Li, Y.-X. Liu, and J.-F. Mao, "A miniature wideband active magnetic probe design with high spatial resolution and high sensitivity for near-field measurement," *IEEE Microw. Wireless Technol. Lett.*, vol. 33, no. 4, pp. 471–474, Apr. 2023.

[30] J. Wang, Z. Yan, J. Liu, Y. Zhou, C. Fu, and D. Su, "Miniature active differential magnetic field probe with high sensitivity for near-field measurements," *IEEE Trans. Antennas Propag.*, vol. 70, no. 2, pp. 1575–1580, Feb. 2022.

[31] Y. Zhou et al., "A miniaturized ultrawideband active electric probe with high sensitivity for near-field measurement," *IEEE Trans. Instrum. Meas.*, vol. 71, 2022, Art. no. 8003608.

[32] G. Li et al., "Ultrawideband differential magnetic near field probe with high electric field suppression," *IEEE Sensors J.*, vol. 20, no. 14, pp. 7669–7676, Jul. 2020.

[33] Z. Yi et al., "Design and characterization of a dual probe with double-loop structure for simultaneous near-field measurement," *IET Microw. Antennas Propag.*, vol. 16, no. 13, pp. 831–840, 2022.

[34] W. Shao et al., "Simultaneous measurement of electric and magnetic fields with a dual probe for efficient near-field scanning," *IEEE Trans. Antennas Propag.*, vol. 67, no. 4, pp. 2859–2864, Apr. 2019.

[35] L. Wang, D. Nie, L. Cheng, and H. Wang, "A high-sensitivity composite probe capable of simultaneously measuring electric- and magnetic-field components," *IEEE Magn. Lett.*, vol. 14, 2023, Art. no. 2100205.